Disrupted local beta band networks in schizophrenia revealed through graph analysis: A magnetoencephalography study

Minami Tagawa, MD,[1,2] Yuichi Takei, MD, PhD [ORCID],[1]* Yutaka Kato, MD, PhD,[1,3] Tomohiro Suto, MD, PhD,[2] Naruhito Hironaga, PhD,[4] Takefumi Ohki, PhD,[5] Yumiko Takahashi, MD, PhD,[1] Kazuyuki Fujihara, MD, PhD,[1,6] Noriko Sakurai,[1] Koichi Ujita,[7] Yoshito Tsushima, MD, PhD[7] and Masato Fukuda, MD, PhD[1]

Aims: Schizophrenia (SZ) is characterized by psychotic symptoms and cognitive impairment, and is hypothesized to be a 'dysconnection' syndrome due to abnormal neural network formation. Although numerous studies have helped elucidate the pathophysiology of SZ, many aspects of the mechanism underlying psychotic symptoms remain unknown. This study used graph theory analysis to evaluate the characteristics of the resting-state network (RSN) in terms of microscale and macroscale indices, and to identify candidates as potential biomarkers of SZ. Specifically, we discriminated topological characteristics in the frequency domain and investigated them in the context of psychotic symptoms in patients with SZ.

Methods: We performed graph theory analysis of electrophysiological RSN data using magnetoencephalography to compare topological characteristics represented by microscale (degree centrality and clustering coefficient) and macroscale (global efficiency, local efficiency, and small-worldness) indices in 29 patients with SZ and 38 healthy controls. In addition, we investigated the aberrant topological characteristics of the RSN in patients with SZ and their relationship with SZ symptoms.

Results: SZ was associated with a decreased clustering coefficient, local efficiency, and small-worldness, especially in the high beta band. In addition, macroscale changes in the low beta band are closely associated with negative symptoms.

Conclusions: The local networks of patients with SZ may disintegrate at both the microscale and macroscale levels, mainly in the beta band. Adopting an electrophysiological perspective of SZ as a failure to form local networks in the beta band will provide deeper insights into the pathophysiology of SZ as a 'dysconnection' syndrome.

Keywords: beta band, graph theory, magnetoencephalography, resting-state network, schizophrenia.

http://onlinelibrary.wiley.com/doi/10.1111/pcn.13362/full

Schizophrenia (SZ) is considered one of the most debilitating psychiatric disorders, owing to the profound cognitive dysfunction associated with this condition. Although numerous studies have helped elucidate the pathophysiology of SZ, many aspects of the mechanism underlying psychotic symptoms remain unknown. Interestingly, alterations in neural activity in certain neurophysiological circuits of the brain have been observed to induce pathological symptoms, such as disconnection syndrome[1–4] and cognitive impairment.[5,6]

This disconnection hypothesis adds the perspective of large cortical networks to the pathophysiology of SZ. First proposed in the 19th century, this hypothesis emphasized that reduced interactions among brain regions may result from abnormal axonal connections.[3] This concept was recently revived because of the important contributions of Friston and Frith.[1] Pettersson-Yeo *et al.* reviewed evidence from emerging functional magnetic resonance imaging (fMRI) studies, which showed reduced functional interactions among brain regions identified by the correlation of blood oxygenation level-dependent signals.[7] Subsequently, Uhlhaas *et al.* modified the original term disconnection ('dis' = 'apart') to *dysconnection* to emphasize

that functional and anatomical connectivity are not generally reduced, but may also involve abnormal increases in SZ ('dys' = 'bad,' 'disease').[8] Indeed, a review of EEG/magnetoencephalography (MEG) studies of the resting-state network (RSN) in SZ showed inconsistent connectivity strength patterns of increased, decreased, and non-significant effects ranging from delta through to gamma for both source-level and sensor-level analysis methods.[9] Despite the inconsistency in connectivity strength changes, SZ consistently exhibits psychotic symptoms, such as positive and negative symptoms. Therefore, we considered the change of 'architecture' of the connectivity of the RSN; that is a topological change in RSN is more important for symptom formation rather than individual connectivity strength change among brain regions in the pathophysiology of SZ.

Recently, the concept of functional templates has been developed.[10] A functional template is a partial connectivity set of RSN that expects or processes upcoming stimuli and events, both with and without explicit stimuli or tasks. This concept is based on studies using fMRI that showed that the RSN typically remains unchanged once a task begins, and that the RSN correlates with perceptual and

behavioral performance.[11] The interactions between neural activities in brain regions formed at various frequencies in the resting state act as functional templates in the resting state and task-related activities.[12] Previous studies have shown that whole-brain network structures across dozens of task states are very similar to the RSN structures.[11] This suggests the existence of a functional template that serves as the standard architecture for functional brain organization. Furthermore, the small but consistent changes that were common across tasks suggest the existence of a task-general network architecture that distinguishes between task and resting states.[12] These results indicate that the functional network architecture during task execution is primarily shaped by functional templates that also exist at rest, and secondarily by evoked task-general and task-specific network changes. This indicates a strong relationship between the RSN and functional connectivity evoked during the task. These mechanisms are thought to be responsible for cognitive functioning,[10] and indeed, results have been obtained correlating RSN with perceptual and behavioral performance.[13,14]

Patients with SZ show deficits in extensive cognitive domains,[15] which may be due to changes in the network structure that lead to various cognitive functions. There are several reports on cognitive functions and network changes in SZ.[16,17] These findings suggest that the symptoms of SZ may be interpreted as a disruption of the functional template resulting from abnormal interactions among brain regions. We postulated that 'dysconnection' in SZ is related to the disruption of the functional template, and that it is important to assess the functional template of RSN.

Owing to the complicated structure of the RSN, it is not possible to quantify the properties that reflect the entire picture by comparing the strength of connectivity among brain regions. Therefore, an advanced analysis is required to quantify the characteristics that reflect the entire picture of the RSN. The present study used a graph theory-based analysis, which has provided insights into topological characteristics, such as the imbalance between local and distributed interactions in the SZ.[18,19] A graph, a mathematical representation of the network, consists of vertices (nodes) and edges (also called links). In this case, the vertices correspond to brain regions, and edges represent connections or statistical dependencies between vertices.[20] Several measures were used to characterize the graphs. The path length is the most commonly used parameter. A path is a trial in which all vertices are distinct, and the path length expresses the paths through which the information travels from one vertex to the remote vertices. The shortest path length is that with the minimum number of edges between two vertices. By applying graph theory to the analysis of brain networks, we were able to evaluate microscale indices, and thus observe how brain activation forms clusters and how these focus on a particular region, and macroscale indices, which reflect the quality and degree of local and global connections of the entire brain.

In this study, microscale indices such as degree centrality (*DG-CENT*) and clustering coefficient (*C-COEF*) were used to indicate how the vertex (a marked point on the cortex) is functionally connected to other vertices. *DG-CENT* represents the number of edges on the vertex, indicating the importance of the vertex in the brain network. *C-COEF* is calculated based on the number of edges between neighboring vertices around the vertex, and *C-COEF* indicates the local cluster coefficient but not the mean clustering coefficient in this study. The term 'neighboring vertices' refers to other vertices that are connected to that vertex. *C-COEF* is a representative measure of functional segregation, the ability of specialized processing within densely interconnected groups of brain regions.[20] Macroscale indices include local efficiency (*LOC-E*), global efficiency (*GLOB-E*), and small-worldness (*SWN*). *GLOB-E* expresses the efficiency of information transfer to the entire network. *LOC-E* reveals how much the system is fault-tolerant; thus, it measures the efficiency of communication between the neighbors of a node when the node is removed.[21] While random networks are characterized by weak clustering and high global integration, a network with a high *SWN* is characterized by strong clustering and high global integration.[22]

Studies using MEG, with a temporal resolution of milliseconds, can identify local and long-range changes in differentiated neural synchronization patterns. MEG addresses the discriminated frequency range that fMRI cannot capture,[23–26] because it detects fast rhythmic fluctuations in activity with periodicity in multiple frequency bands, ranging from <1 Hz to well above 100 Hz. In recent years, there have been some reports of an association between resting activity, differentiated by carrier frequency, and gamma-amino butyric acid levels assessed by magnetic resonance spectroscopy (MRS). The carrier frequency of the RSN has different physiological implications, such as neurotransmitter concentration, and provides key information for understanding the pathology of SZ.[27–29] Recently, MEG analysis tools have remarkably improved,[30,31] and the MEG oscillatory network is comparable to the fMRI network.[23,24] The results of previous fMRI studies have increased the credibility of resting networks analyzed by MEG. In addition, a higher temporal resolution than fMRI allows for more detailed frequency analysis. However, few studies have analyzed the resting network in SZ using MEG,[32–36] and only one study investigated the topological characteristics of SZ using graph analysis.[37] Their study had a small sample size, calculated network connectivity by the coherence method without source leakage correction, and evaluated only limited types of graph metrics (degree, path length, and small-worldness).

In this study, we hypothesized that psychotic symptoms in SZ originate from changes in the topological characteristics of local and global networks across different frequency bands and evaluated the topological characteristics of local and global networks in patients with SZ and their relationship with psychotic symptoms.

Methods

Participants

Forty-three patients with SZ and 38 healthy controls (HCs) were recruited from Gunma University Hospital, Japan (Table 1) between September 2014 and February 2020. This study was approved by the ethics committee of the Gunma University Hospital. After a detailed description of the study, each participant provided written informed consent before the start of the study. This study was conducted according to the principles of the Declaration of Helsinki. We used the Edinburgh Handedness Inventory to ensure that all the registered participants were right-handed.[38] To diagnose SZ and exclude participants with a history of psychiatric disorders from the HCs, we conducted the Structured Clinical Interview for DSM Disorders, 4th Edition Axis I[39] and Axis II Disorders.[40] Psychopathology ratings were obtained using the Positive and Negative Syndrome Scale (PANSS),[41] Japanese Adult Reading Test (JART),[42] and Global Assessment of Functioning (GAF).[43] We calculated the chlorpromazine equivalent dose of antipsychotics for SZ.[44] Details of the recruitment of participants are provided in the Appendix S1.

MEG data acquisition and preprocessing

We acquired 7 min of MEG data for each patient. The only instructions for participants were to relax with their eyes open, gazing at a fixed point, and to remain awake in an upright position during acquisition. MEG data were acquired inside a magnetically shielded room (JFE Mechanical Co., Tokyo, Japan) using a 306-channel Elekta NeuroMag (Oy, Helsinki, Finland).

We used the Stanford Sleepiness Scale[45] to evaluate the extent of sleepiness (i.e. check awake levels) during MEG acquisition. There was no significant difference in sleepiness between the SZ and HC groups (median, interquartile range: 3.0, 2.0–4.0 vs 3.0, 3.0–4.0, z-score = −0.386, P = 0.3445). Data from 14 SZ patients were excluded owing to excessive artifacts (5 SZ), interruption of MEG measurement (4 SZ), and failure of FreeSurfer reconstruction (5 SZ), resulting in a final sample of 29 SZ patients (Table 1).

For preprocessing, we applied the 'oversampled temporal projection 'method, signal space separation method,[46,47] notch filter, and independent component analysis (ICA) to the sensor data (Fig. 1a).

Table 1. Participant characteristics

	SZ		HC		χ^2	P
	Total cases $n = 43$ Dropped cases $n = 14$ Survived cases $n = 29$		Total cases $n = 38$ Dropped cases $n = 0$ Survived cases $n = 38$			
	M	F	M	F	0	1
Sex (male)	12	17	16	22		
	Mean	SD	Mean	SD	t	P
Age (year)	40.8	6.7	40.4	6.1	−0.249	0.8038
Age range (year)	28–52		29–55			
JART	105.4	12	110.8	7.2	2.325	0.0232*
GAF	48.1	11.3				
PANSS	Mean	SD				
Positive symptoms	13.6	5.8				
Negative symptoms	19.0	7.9				
General psychopathology	31.3	11.0				
Total score	63.8	22.6				
Medications		Mean	SD	n		
Antipsychotic (chlorpromazine equivalent dose mg/day)		451.0	414.7	24		
Antidepressant (imipramine equivalent dose mg/day)		2.6	14	2		
Anxiolytic (diazepam equivalent dose mg/day)		0.7	3	2		
Hypnotic (flunitrazepam equivalent dose mg/day)		0.6	0.9	11		

*Indicate statistically significant results: $P < 0.05$.
GAF, Global Assessment of Functioning; HC, healthy controls; JART, Japanese Adult Reading Test; PANSS, Positive and Negative Syndrome Scale; SZ, schizophrenia patients; SD, standard deviation.

The details of data acquisition and preprocessing are described in the Appendix S1.

MEG source imaging

We applied a source localization analysis to MEG time-series data by using the minimum norm estimates (MNE) suite and MNE Python.[48] The FreeSurfer reconstruction process was used to generate individual T1-weighed MRI data (details of scanning are provided in the Appendix S1) and cortical reconstructions for each participant.[49–51] The boundary element method using a single compartment surrounded by the inner surface of the skull was used for head modeling.[52] Noise-normalized dynamic statistical parameter mapping was further applied to estimate the current source waveform using the noise covariance matrix created from the entire empty room measurement.[53]

Connectivity analysis for RSNs

The schematic images of the data analysis procedure used in this study are shown in Fig. 1. First, source distribution was evaluated using the aforementioned method (Fig. 1a). We then acquired the morphed source distribution using 'fsaverage' and the reconstructed brain surface was decimated to 1000 vertices (Fig. 1b). One of the major problems in estimating connectivity in MEG analysis is source leakage.[54] There are two ways to deal with this problem: using source leakage-independent indices, such as imaginary coherence and the phase lag index, or using orthogonalized amplitude envelope correlation.[55] The former results from the phase coupling of band-limited oscillating signals, whereas the latter results from the coupling of aperiodic fluctuations of the signal envelope per frequency band. Functional coupling provides a tuning window for spatially separated

neuronal populations to increase or decrease excitability, and both approaches reflect similar intrinsic functional connectivity.[56] Evaluation by envelope correlation is thought to adjust on a longer timescale, whereas phase coupling adjusts on a faster timescale. In our study, we used orthogonalized envelope correlations, as we thought it would be more suitable for assessing consistent patterns of the resting state network and not for assessing transient network formation, such as stimulus-related changes. Furthermore, the orthogonalized envelope correlation showed the most stable results from the viewpoint of group-level repeatability, within-subject consistency, and between-subject consistency in previous studies that examined the stability of connectivity assessment.[57] We applied source leakage correction to MEG data using 'envelope correlation' that was implemented in MNE python[24,58] at delta (1–4 Hz), theta (4–8 Hz), alpha (8–12 Hz), low beta (13–20 Hz), high beta (20–30 Hz), and gamma (30–80 Hz) bands (Fig. 1c). The high beta band (20–29 Hz) is sometimes included as part of the gamma band in data analysis, and the basic inhibition-based mechanisms underlying gamma rhythms have been shown experimentally to extend into this range.[59] Therefore, we divided the beta band activity into low-and high-beta bands. The details of the formula for the orthogonal envelope correlation are provided in the Appendix S1. After calculating the median sliding correlation values (Fig. S1), graph theory analysis was performed on these values, as described below.

Graph analysis

The connectivity matrices were evaluated using undirected graph analysis as both microscale and macroscale indices to characterize the RSN in each frequency band. The details of the formula for the graph-theoretical measures are provided in the Appendix S1. In this graph analysis,[20–22,60–63] each brain region where the source time
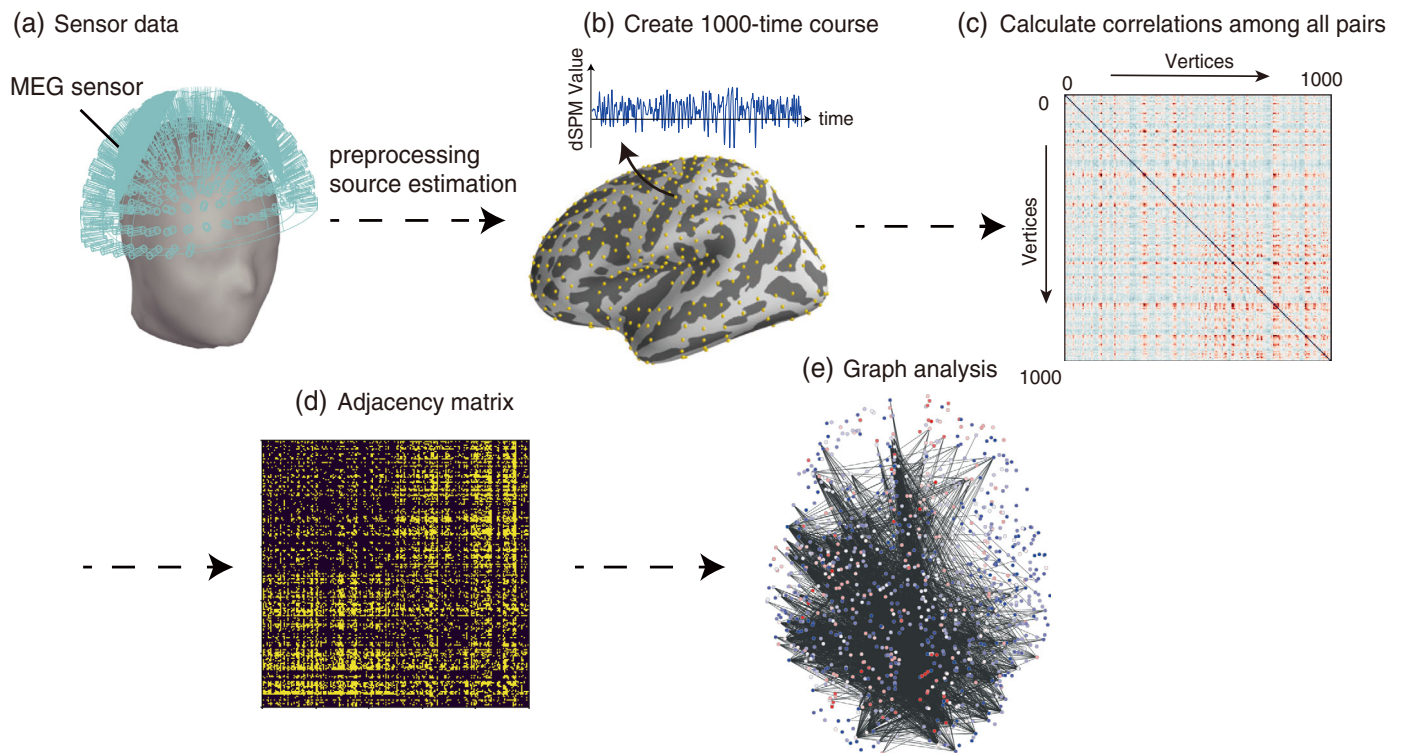
Fig.1 A scheme of the analysis flow. (a) Starting from sensor detections from 306-ch MEG. (b) The source distribution image was estimated using MNE, and source waveforms were extracted from 1000 vertices. (c) The correlation of the power envelopes of the corrected source waveforms. (d) The threshold level in the correlation matrix was adjusted, ranging from 5 to 30% in increments of 5%; all parameter settings, such as the density or number of connections of the network, were identified across all individuals. (e) The graph matrices were calculated from adjacency matrices. MEG, magnetoencephalography; MNE, minimum norm estimates.

course was acquired was defined as a vertex, and the binarized connectivity between vertices was defined as an edge. A connectivity matrix A, which included orthogonal correlations between all $N \times N$ vertex pairs ($N = 1000$ in the present case) at each frequency band (we used six frequency ranges as described in subsection Connectivity analysis for resting-state networks), was calculated for each subject to apply graph theory to the extracted source waveform. Next, an adjacency matrix B, consisting of binarized connectivity indices (i.e. edges), was calculated over a threshold range of 5–30% in increments of 5% (six steps) to evaluate the topological indices. Matrix B was used to ensure an equal number of edges for all the participants (Fig. S2, Table S1). We then computed the topological characteristics of the microscale, *DG-CENT*, and *C-COEF*. *DG-CENT* is a simple centrality measure that counts the number of neighboring vertices that are present. *C-COEF* measures the clustering of vertices in a graph. The *C-COEF* of a vertex can be evaluated by calculating the number of neighboring vertices that are connected to each other. Triangles are formed when adjacent vertices are connected. The degree of clustering can be evaluated by taking the ratio of the number of triangles to the maximum possible number of triangles centered on the vertex.

Next, we calculated the topological characteristics at the macroscale (*GLOB-E*, *LOC-E*, and *SWN*). *GLOB-E* measures provide an indication of how effectively information is integrated throughout the network and is related to the average inverse shortest path length in the network. *LOC-E* provides an indication of how effectively information is integrated among the nearest neighboring vertices of a given network vertex and indicates how efficiently neighboring vertices can communicate once a vertex is removed. Small-world networks are a class of networks that are highly clustered, similar to regular lattice graphs, and have an average shortest path length similar to random graphs.[62] A lattice graph is a graph in which the vertices are such that each vertex connects to the subsequent vertices, which are exactly one unit away from it, and is

characterized by high clustering. A random graph is a graph in which the connections between vertices are determined randomly, and the graph is characterized by a low shortest path length. *SWN* is a measure of the balance between local and global connections.[60] The *SWN* is measured by the mean *C-COEF* across all vertices and the average shortest path length, L.

Statistical analyses

We compared the graph theory indices between the HC and SZ groups using the Mann–Whitney rank test in SciPy[64] because the distribution of the graph indices indicated a non-Gaussian distribution. We applied a false discovery rate correction (FDR) to the P-values of *DG-CENT* and *C-COEF* for the number of frequencies (6) × number of thresholds (6) × number of vertices (1000) and to the p-values of GLOB-E, LOC-E, and SWN for the number of frequencies (6) × number of thresholds (6) to avoid type 1 errors.[65]

A multiple stepwise linear regression analysis was conducted to examine the relationship between significantly different graph indices in SZ and clinical measures. Before the regression analysis, we investigated the partial correlation between independent factors. The results showed a high correlation between sleepiness before and during the measurements ($r = 0.683$, $P = 0.0001$). We also found a high correlation between LOC-E and GLOB-E ($r = 0.500$, $P = 0.0068$ at the low beta band), and LOC-E and SWN ($r = 0.999$, $P < 0.0001$ at the low beta band) were also highly correlated. Therefore, we conducted three models using any one of graph index (GLOB-E, LOC-E, or SWN) as independent variables to avoid multicollinearity. We used clinical measures (PANSS and GAF) as dependent variables and graph index, sex, age, the dosage of antipsychotics, sleepiness during measurement, and JART as independent variables in this multiple regression analysis. Variables were excluded based on the Akaike information criterion (AIC) to select the model with the minimum AIC.

Results

Original correlation matrix

First, we describe the original correlation matrix and provide an overview of the differences between the SZ and HC groups (Fig. S1). Connectivity of the two groups showed similar distributions for each frequency band. The correlation values at each threshold of the SZ group were lower than those of the HC group in the alpha and low beta bands (Table S1). However, there were no significant differences in the delta, theta, and gamma bands.
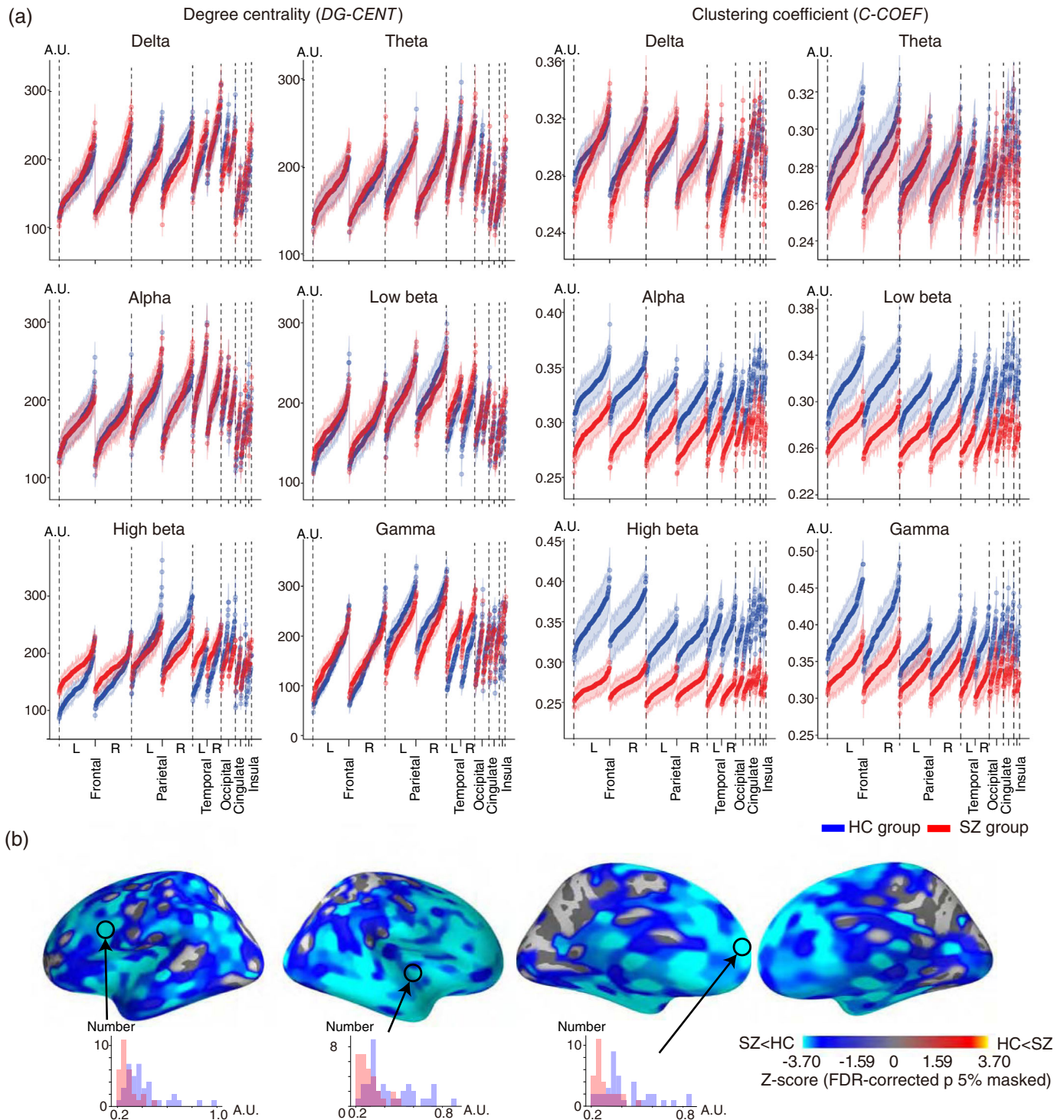

Fig.2 Topological characteristics of the vertex level. (a) *DG-CENT* and *C-COEF* of the HC group (blue) and the SZ group (red) at thresholding 20%. The two columns on the left indicate *DG-CENT*, and the two columns on the right indicate *C-COEF* at each frequency band. The circles (blue or red) indicate median values of each index, and the translucent bands indicate standard error. Each figure is separated by brain regions with dashed lines. The black squares indicated the *C-COEF* that showed a remarkable difference between HC and SZ. (b) Distribution of the z-scores calculated using Mann–Whitney U-test of the *C-COEF* between the HC and SZ groups at the high beta band at a threshold of 20%. The regions that showed significant differences are colored blue or yellow-red under FDR-corrected p 5%. The blue regions indicate that the SZ group has significantly lower values than the HC group. Histogram plots show the clustering coefficients of each group (HC group; blue, SZ group; red) at the vertex pointed by the arrow. A.U., arbitrary unit; *C-COEF*, clustering coefficient; *DG-CENT*, degree centrality; FDR, false discovery rate; HC, healthy control; l, left; r, right; SZ, schizophrenia.

Table 2. Topological characteristics of the microscale at the 20% threshold

		HC median (IQR)	SZ median (IQR)	Number of the vertices under significant level
DG-CENT	Delta	180.0 (125.0 to 252.0)	180.0 (124.0 to 252.0)	0
	Theta	183.0 (127.0 to 254.0)	182.0 (132.0 to 248.0)	0
	Alpha	181.0 (111.0 to 272.0)	182.0 (125.75 to 255.0)	0
	Low beta	177.0 (123.0 to 251.0)	185.0 (135.0 to 247.0)	0
	High beta	174.0 (115.0 to 254.0)	185.0 (137.0 to 244.0)	0
	Gamma	176.0 (106.0 to 267.0)	184.0 (118.0 to 262.0)	0
C-COEF	Delta	0.292 (0.26 to 0.335)	0.289 (0.247 to 0.338)	6
	Theta	0.284 (0.248 to 0.338)	0.274 (0.241 to 0.329)	2
	Alpha	0.325 (0.278 to 0.38)	0.29 (0.251 to 0.339)	155
	Low beta	0.309 (0.267 to 0.371)	0.272 (0.241 to 0.318)	254
	High beta	0.338 (0.282 to 0.443)	0.27 (0.238 to 0.32)	850
	Gamma	0.378 (0.311 to 0.475)	0.332 (0.285 to 0.398)	65

		Mann to Whitney rank test		
		U value ranges of all vertices	Z-score ranges of all vertices	FDR-corrected P ranges of all vertices
DG-CENT	Delta	222.5 to 825.0	−4.157 to 3.467	0.052 to 1.0
	Theta	270.5 to 799.0	−3.55 to 3.138	0.08 to 1.0
	Alpha	346.0 to 761.0	−2.594 to 2.657	0.172 to 1.0
	Low beta	275.5 to 829.0	−3.486 to 3.518	0.08 **to** 1.0
	High beta	205.5 to 896.0	−4.372 to 4.366	0.052 to 1.0
	Gamma	235.0 to 891.5	−3.999 to 4.309	0.052 to 1.0
C-COEF	Delta	303.0 to 727.0	−3.138 to 2.227	0.019* to 0.996
	Theta	333.0 to 686.0	−2.759 to 1.708	0.037* to 0.996
	Alpha	209.0 to 580.0	−4.328 to 0.367	0.006** to 0.991
	Low beta	214.0 to 556.0	−4.265 to 0.063	0.006** to 0.973
	High beta	174.0 to 530.0	−4.771 to −0.266	0.006** to 0.869
	Gamma	289.0 to 575.0	−3.315 to 0.304	0.013* to 0.996

*Indicate statistically significant results: FDR-corrected $P < 0.05$.
**Indicate statistically significant results: FDR-corrected $P < 0.01$.
C-COEF, clustering coefficient; *DG-CENT*, degree centrality; FDR, false discovery rate; HC, healthy controls; IQR, interquartile range; SZ, schizophrenia patients.

Topological characteristics of microscale indices

First, we compared *DG-CENT* and *C-COEF* as the topological characteristics of the microscale indices to investigate the differences in the characteristics of each vertex between the HC and SZ groups (Fig. 2, Table 2).

There was no significant difference in *DG-CENT* between the SZ and HC groups on the vertices in any frequency band (Fig. 2a, left). However, significant differences were clearly observed in the *C-COEF* at the 20% threshold between the SZ and HC groups, especially in the alpha,

(a) Topological characteristics of the mesoscale indices
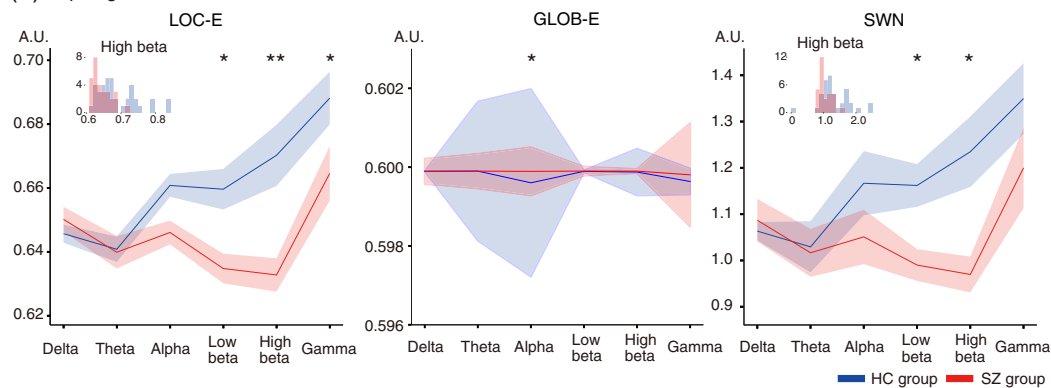
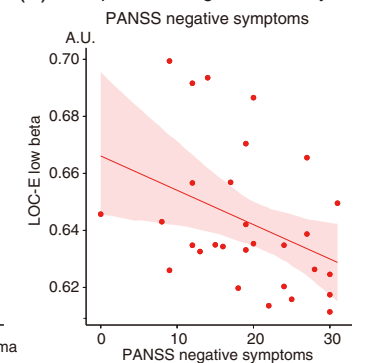**(b)** Multiple linear regression analysis

Fig.3 Topological characteristics of the macroscale and Spearman's rank correlation between graph indices and clinical measures. (a) Local efficiency and *SWN* of SZ and HC groups at the 20% threshold. The solid lines indicate the median value of each index, and the translucent bands indicate standard error. Histogram plots show the distribution of graph indices of each group at frequency bands that showed significant differences. *FDR-corrected $P < 0.05$; **FDR-corrected $P < 0.01$. (b) Scatter plot of the significant results of a multiple stepwise linear regression analysis to assess the relationship between graph indices and clinical measures in the SZ group. Translucent bands indicate a 95% confidence interval for the regression estimate. A.U., arbitrary unit; PANSS, Positive and Negative Syndrome Scale; *LOC-E low beta*, local efficiency; SZ, schizophrenia.

low-beta, high-beta, and gamma bands (Fig. 2a, right). Only small differences were observed in the delta-and theta-band ranges. Figure 2b (see also Fig. S3) shows the distribution of the z-scores masked by the FDR-corrected P-value below 5%; the decrease in C-COEF of the SZ group was apparent in the frontal and temporal regions.

Topological characteristics of macroscale indices

Next, we identified three graph theory metrics (*GLOB-E*, *LOC-E*, and *SWN*) (Fig. 3) to investigate the function and nature of the entire network. Each graph measure is shown in Fig. 3a and Table 3 at a 20% threshold, and in Tables S2–S6 at all thresholds. These tables show the consistency of our results across a range of thresholds. There were significant differences in LOC-E and SWN between the SZ and HC

groups, particularly in the alpha, low-beta, and high-beta bands. The LOC-E of the SZ group was significantly lower than that of the HC group in the low-beta, high-beta, and gamma bands. *The SWN* in the SZ group was significantly lower than that in the HC group in the low-and high-beta bands. However, GLOB-E in the alpha band in the SZ group was significantly higher than that in the HC group. The distribution of *GLOB-E* showed a specific pattern in which almost all data were approximately 0.60 in both groups.

Relationship between graph index characteristics and clinical symptoms

A multiple stepwise linear regression was calculated to predict clinical measures (PANSS and GAF) based on LOC-E at the 20%

Table 3. Topological characteristics of the macroscale at the 20% threshold

		HC median (IQR)	SZ median (IQR)
GLOB-E	Delta	0.5999 (0.59989–0.5999)	0.59989 (0.59987–0.5999)
	Theta	0.5999 (0.59962–0.5999)	0.5999 (0.59989–0.5999)
	Alpha	0.5996 (0.59832–0.59986)	0.59989 (0.59964–0.5999)
	Low beta	0.59989 (0.59983–0.5999)	0.5999 (0.59987–0.5999)
	High beta	0.59988 (0.59981–0.5999)	0.5999 (0.59989–0.5999)
	Gamma	0.59964 (0.59906–0.59986)	0.59981 (0.59953–0.59988)
LOC-E	Delta	0.646 (0.64–0.66)	0.65 (0.631–0.656)
	Theta	0.641 (0.624–0.656)	0.64 (0.624–0.657)
	Alpha	0.661 (0.644–0.669)	0.646 (0.632–0.661)
	Low beta	0.66 (0.638–0.676)	0.635 (0.626–0.657)
	High beta	0.67 (0.649–0.729)	0.633 (0.625–0.66)
	Gamma	0.688 (0.672–0.734)	0.665 (0.65–0.695)
SWN	Delta	1.062 (1.02–1.167)	1.086 (0.944–1.13)
	Theta	1.028 (0.902–1.11)	1.015 (0.886–1.143)
	Alpha	1.166 (0.986–1.228)	1.05 (0.913–1.183)
	Low beta	1.161 (1.007–1.29)	0.989 (0.918–1.139)
	High beta	1.234 (1.054–1.643)	0.968 (0.913–1.191)
	Gamma	1.348 (1.213–1.68)	1.199 (1.079–1.417)

	Mann–Whitney rank test		
	U value ranges of all vertices	*Z*-score ranges of all vertices	FDR-corrected *P* ranges of all vertices
GLOB-E	Delta	454	−1.227	0.333
	Theta	577.5	0.335	0.83
	Alpha	785	2.961	0.046*
	Low beta	711.5	2.031	0.094
	High beta	715.5	2.082	0.09
	Gamma	660.5	1.386	0.263
LOC-E	Delta	499	−0.658	0.618
	Theta	535	−0.202	0.921
	Alpha	384	−2.113	0.062
	Low beta	328	−2.822	0.016*
	High beta	259	−3.695	0.001**
	Gamma	357	−2.455	0.034*
SWN	Delta	472	−1	0.444
	Theta	538.5	−0.158	0.904
	Alpha	450	−1.278	0.333
	Low beta	330	−2.797	0.028*
	High beta	293	−3.265	0.013*
	Gamma	377	−2.202	0.072

*Indicate statistically significant results: FDR-corrected $P < 0.05$.
**Indicate statistically significant results: FDR-corrected $P < 0.01$.
FDR, false discovery rate; *GLOB-E*, global efficiency; HC, healthy controls; IQR, interquartile range; *LOC-E*, local efficiency; *SWN*, small-worldness; SZ, schizophrenia patients.

Table 4. The results of a multiple stepwise linear regression analysis

	Beta	SE	T	P value
PANSS negative symptoms				
LOC-E low beta	−2.9331	1.376	−2.131	0.042*
Intercept	18.9655	1.376	13.779	0
VIF factors				
Age	JART	Antipsychotic	Sleepiness during task	LOC-E low beta
1.247	1.094	1.066	1.14	5.712

*Indicate statistically significant results: $P < 0.05$.
The independent variables (sex, age, dosage of antipsychotics, sleepiness during measurement, and JART) were removed during analysis processing.
JART, Japanese Adult Reading Test; LOC-E low beta, local efficiency at low beta band; PANSS, Positive and Negative Syndrome Scale; SE, standard error; VIF factors, variance inflating factors.

threshold, sex, age, antipsychotic drug dosage, sleepiness during measurement, and JART. A significant regression equation including LOC-E was found regarding the negative symptoms of PANSS (F (1, 27)=4.541, $P = 0.0424$), with an R2 of 0.144 at the low beta band (Table 4). There was no significant relationship with other clinical measures at the low beta band and with all clinical measures at the alpha, high beta, and gamma bands. Negative symptoms of PANSS were equal to 18.966–2.9331 × LOC-E $_{low\ beta}$, and LOC-E at the low beta band was a significant predictor of negative symptoms of PANSS. In contrast, age, antipsychotic drug dosage, sleepiness during measurement, and JART were not significant predictors of psychotic symptoms. There was no significant regression equation including GLOB-E or SWN.

Discussion

In the present study, we investigated the topological characteristics of RSNs from the viewpoint of local and global networks in patients with SZ, and their relationship with psychotic symptoms using graph theory. At the microscale level, the results confirmed our hypothesis that patients with SZ presented a lower *C-COEF* in the beta band, mostly in the frontal and temporal regions. At the macroscale, the *LOC-E* and *SWN* values of the low-and high-beta bands were clearly reduced in the SZ group. To our knowledge, this is the first study to show that there are remarkable topological changes in the RSN of the beta band in the SZ. Below, we consider these results in the context of their associated pathophysiological mechanisms and how they may be interpreted within the context of current neuroscientific findings.

Alternation of the topological characteristics in SZ compared to HC

A significant difference in *C-COEF*, but not in *DG-CENT*, was observed between the SZ and HC groups. The decrease in *C-COEF* in the SZ group was consistent with those found in previous resting-state fMRI studies.[66,67] Although *C-COEF* showed significant differences between the SZ and HC groups, *DG-CENT* showed almost identical results with no significant differences between these groups (Fig. 2a, left), indicating that alterations in the neural network of patients with SZ did not originate from changes in the number of connections at each vertex but from the change in the relationship of connections with other vertices.

C-COEF is a topological index that evaluates the local network function. It is important to note that 'local' in this case does not refer to co-localized brain regions but rather to vertices that are located close to each other in the network. C-COEF implies that the edges between vertices are connected to one vertex and represents local special abilities as a set of partial connectivity in the RSN. Although the

concept of functional templates and structure of RSN has not been well-mapped, functional templates are believed to be represented by a set of connectivities across different brain regions, rather than a specific brain region, and clustered networks are a form of functional template. Therefore, the C-COEF observed in the RSN can be regarded as an indicator of a functional template. The functional template is a standard architecture for the functional organization of the brain and contributes to the realization of cognitive functions, as indicated by the correlation between RSNs and perceptual and behavioral performance.[13,14] The C-COEF of the RSN is also considered an important indicator of the organization of complex brain functions.

In addition, LOC-E is a topological index that assesses the local network function at the macroscale level. LOC-E is calculated by the average efficiency of the network consisting of the nearest neighboring vertices and provides an indication of how effectively information is integrated among the nearest neighboring vertices of a given network vertex. The concept of LOC-E is interpreted to be the same as the mean clustering coefficient of the entire brain.[63] In other words, LOC-E evaluates the extent to which functionally segregated templates are formed throughout the brain. Combined with previous findings, these results suggest the possibility of network reconstruction, especially at the local level, in patients with SZ.[66–73] This could indicate the destruction of the functional templates that underlie cognitive functions, thus implicating the extent of 'dysconnection.' We also found that the SZ group had lower *SWN* in the beta band than the HC group (Fig. 3a). The lower *SWN* at the low and high beta bands in the SZ group indicates a less optimal organization of the RSN in SZ. Because the *SWN* was calculated by dividing the averaged *C-COEF* by the average shortest path length, the inefficiencies of the local network are likely to affect the optimization of the entire RSN.

Topological alterations were mostly observed in the high beta band. Although the neurophysiological implications of high-beta band alterations in the SZ group are not sufficiently understood, some previous studies have associated them with NMDA receptor dysfunction. Models using NMDA receptor antagonists have been used to mimic many of the major symptoms of SZ,[74] and there is evidence that disruption of glutamatergic function is related to SZ.[75,76] As Roopun *et al.* described, the gamma rhythm is not the only rhythm affected in SZ, the high band (20–29 Hz) EEG rhythm deserves particular attention. They examined the relationship between NMDA receptors and high-beta band activity by quantitatively comparing the effects of ketamine on gamma and high-beta band activation. They found that ketamine affected both gamma and high-band activation, but the effects differed among brain regions.[59] Akbarian *et al.* reported changes in the mRNA levels of the NMDA receptor NR2 subunit in the prefrontal cortex of the postmortem brain in SZ.[77] Our findings suggest that the decrease in *C-COEF*, largely observed in the frontal

and temporal regions of the high beta band, could reflect deficits in NMDA receptor-mediated excitatory synaptic activity in the SZ group.

While we found a changed network of the SZ group at high-frequency bands, we could not find a significant change at low-frequency bands such as theta or delta. Khan *et al.* reported changes in frequency band-specific maturation of RSNs from age 7 to 29 and found changes in graph indices from childhood to adulthood in the beta and gamma bands.[58] They found increased LOC-E and *SWN* in the beta band, increased GLOB-E, and decreased *SWN* in the gamma band. In other words, they report opposite developmental trajectories of segregation at the beta band and integration in the gamma band. However, they found no age-related changes in low-band frequency networks, such as delta and theta. We speculate that these results may be due to the low-frequency network structures reaching completion at a relatively young age compared to the high-frequency network structures. It is well known that SZ develops from adolescence to adulthood, which may mean that high-frequency network structures are more susceptible to pathophysiological changes in SZ at the developmental stage. In contrast, low-frequency networks that form early in life may be less susceptible to pathophysiological changes in patients with SZ. Although we only investigated patients with SZ in this study, comparing patients with SZ and at-risk mental states of SZ may shed light on the meaning of these frequency-specific graph changes.

Alternation of topological characteristics related to psychotic symptoms in the SZ group

In the SZ group, the LOC-E of the low beta band was negatively correlated with the negative symptoms (Fig. 3b). There is a wide range of negative symptoms in patients with SZ, including emotional and cognitive characteristics, such as blunted affect, lack of spontaneity, and difficulty in abstract thinking. The fact that LOC-E is correlated with negative symptoms indicates that failure to form a well-integrated local network as a functional template actually represents an SZ symptom.

Wang *et al.* compared the functional neural network in the SZ group at baseline during the first episode and after 4 months of treatment with antipsychotics.[69] They found a lower average clustering coefficient and LOC-E in the first episode in the SZ group than in the HCs and that these changes were modulated by treatment with antipsychotic drugs. Longitudinally, negative symptoms improved as the average clustering coefficient increased, suggesting that antipsychotics could help remedy the disorganized local network seen in the SZ group. Furthermore, the average clustering coefficient reflects the local clustering of topological organization, similar to LOC-E, suggesting that it may be a marker of therapeutic responsiveness to second-generation antipsychotics in patients with SZ. Consistent with these studies, LOC-E is a promising index for assessing the psychotic symptoms of SZ.

Previous studies on MEG on RSNs in patients with SZ

Several studies have investigated the resting connectivity of the SZ using MEG.[32–37,78,79] Many of these studies have investigated the strength of connectivity between brain regions but have not focused on the characteristics of the network using graph analysis. Rutter *et al.* investigated the differences in topological characteristics between HC and SZ groups using MEG.[37] However, group differences in the global graph metrics showed no statistical significance after multiple comparisons. They described their findings as unexpected and questioned whether the graphs derived from MEG in their study are meaningful in relation to brain processes, due to the small number of subjects and the choice of coherence as a measure of functional connectivity. They stated that source-level connectivity measures in MEG may yield artifacts strong enough to render the graphs meaningless,[80] or they may be consistent with whole-brain connectivity studies that have shown consistency between fMRI and MEG

results.[23,81] Noise rejection methods used in MEG have grown remarkably in recent years.[82] We performed noise reduction using oversampled temporal projection, Elekta Neuromag Maxfilter, notch filter, and ICA as preprocessing for the connectivity analysis. These methods, developed in recent years, are stronger than the methods of Rutter *et al.*, who rejected epochs with high eye artifacts and head movement of over 0.5 cm, and used only a notch filter and a band-pass filter. The difference in noise reduction methods may be one of the factors causing the discrepancy in results.

Additionally, Rutter *et al.* calculated the connectivity matrix using the coherence method, whereas we used an orthogonalized envelope correlation. As stated in the Methods section, the orthogonalized envelope correlation showed the most stable results in terms of group-level repeatability, within-subject consistency, and between-subject consistency in previous studies that examined the stability of the connectivity assessment.[57] On the other hand, the coherence used by Rutter *et al.* is known to be affected by source leakage,[83] and it must be said that the connectivity matrix in their study used as the basis for graph analysis is unreliable. Envelope correlation can be thought of as fluctuations in acyclic (scale-free) activity with most of the energy at frequencies below 0.1 Hz, reflecting the joint activity of a population of neurons on a slow time scale of a few seconds to a few minutes. Envelope correlation is more likely to represent coherent excitatory fluctuations that alter the activation of brain regions in a coordinated manner. Thus, envelope correlations may modulate the availability of neuronal populations or regions to prepare for subsequent tasks. Functional connectivity provides a window of adjustment for spatially separated neuronal populations to increase or decrease their excitability.[84] This suggests that local dynamics may be regulated on either a slow or fast timescale, depending on whether the envelope or phase connectivity is predominant. The envelope correlation represents coherent excitatory fluctuations that lead to coordinated changes in the activation of brain regions and represents a limited setting of regional availability, with implications that may form the basis of functional templates. In other words, the results of the present study indicate that the network structure, which is normally constrained by a limited setting in the form of a functional template in HCs, is disrupted in SZ, and this is likely linked to psychiatric symptoms.

Conclusions

We investigated the 'dysconnection' symptomatology of the SZ brain *via* graph theory analysis using MEG. We found that local network efficiency was impaired at both the micro- and macroscale levels in SZ brains, especially in the high beta band, indicating that the pathophysiology of SZ is predominantly based on the disturbance of the local network. These topological changes are associated with psychotic symptoms. The 'dysconnection in SZ' observed in our study was due to the disruption of the functional template expressed as the disturbance of the local topological characteristics in the local network.

Limitations

This study had several limitations. One limitation is that we chose to focus on eyes open as our resting state paradigm, rather than eyes closed, thus minimizing the alpha power. This was performed in accordance with the guidelines of the Human Connectome Project. In addition, eyes-open RSNs derived using MEG have greater test–retest reliability than eyes-closed-derived networks.[85] Although some MEG/EEG studies have found differences between the two conditions,[85,86] the overall differences between the eyes closed and eyes open conditions in these studies were small. Our findings provide compelling evidence of topological alternations underlying psychotic symptoms in the SZ group; nonetheless, several experimental designs and methodological issues should be considered. Most patients with SZ receive antipsychotic drugs. We investigated the relationship between topological characteristics and the dose of

antipsychotic medication and found no significant effect on topological characteristics in the current study. However, further comparisons and considerations, including drug-naïve patients, are required to verify our findings. Moreover, there is a potential bias in that most SZ patients who can complete MEG recording and provide adequate data do not have severe or active symptoms.

In this study, we used binarized multi-threshold graph-theoretic measures. Since there is no specific rationale for using cost thresholds, we set the thresholds to range from 5% to 30% in 5% increments to compare the properties of the graph networks over a wide range of costs. However, weighted equivalents have also recently emerged. Weighted graphs are assumed to align more closely with the ground-truth physiology. In the future, we would like to consider weighted graph measures.

We used a 1000 parcellation scheme because cortical surface is very convoluted and averaging across a large label can result in signal cancellation. However previous study indicates functional connectivity estimation may suffer from the presence of spurious interactions[87] and that it was shown that the optimal number of parcels was approximately 70.[88] We cannot conclude whether high-resolution parcellation is appropriate for the graph analysis of MEG, but we consider that this should be verified in the future.

Disclosure statement
The authors declare no conflict of interest.

Author contributions

References

1. Friston KJ, Frith CD. Schizophrenia: A disconnection syndrome? *Clin. Neurosci.* 1995; **3**: 89–97.
2. Friston KJ. Theoretical neurobiology and schizophrenia. *Br. Med. Bull.* 1996; **52**: 644–655.
3. Stephan KE, Friston KJ, Frith CD. Dysconnection in schizophrenia: From abnormal synaptic plasticity to failures of self-monitoring. *Schizophr. Bull.* 2009; **35**: 509–527.
4. Geschwind N. Disconnexion syndromes in animals and man. I. *Brain* 1965; **88**: 237–294.
5. Andreasen NC, Paradiso S, O'Leary DS. "Cognitive dysmetria" as an integrative theory of schizophrenia: A dysfunction in cortical-subcortical-cerebellar circuitry? *Schizophr. Bull.* 1998; **24**: 203–218.
6. Andreasen NC, Nopoulos P, O'Leary DS, Miller DD, Wassnik T, Flaum M. Defining the phenotype of schizophrenia: Cognitive dysmetria and its neural mechanisms. *Biol. Psychiatry* 1999; **46**: 908–920.
7. Pettersson-Yeo W, Allen P, Benetti S, McGuire P, Mechelli A. Dysconnectivity in schizophrenia: Where are we now? *Neurosci. Biobehav. Rev.* 2011; **35**: 1110–1124.
8. Uhlhaas PJ. Dysconnectivity, large-scale networks and neuronal dynamics in schizophrenia. *Curr. Opin. Neurobiol.* 2013; **23**: 283–290.
9. Mackintosh AJ, de Bock R, Lim Z *et al.* Psychotic disorders, dopaminergic agents and EEG/MEG resting-state functional connectivity: A systematic review. *Neurosci. Biobehav. Rev.* 2021; **120**: 354–371.
10. Ohki T, Takei Y. Neural mechanisms of mental schema: A triplet of delta, low beta/spindle and ripple oscillations. *Eur. J. Neurosci.* 2018; **48**: 2416–2430.
11. Foster BL, Rangarajan V, Shirer WR, Parvizi J. Intrinsic and task-dependent coupling of neuronal population activity in human parietal cortex. *Neuron* 2015; **86**: 578–590.
12. Cole MW, Bassett DS, Power JD, Braver TS, Petersen SE. Intrinsic and task-evoked network architectures of the human brain. *Neuron* 2014; **83**: 238–251.
13. Provost JS, Monchi O. Exploration of the dynamics between brain regions associated with the default-mode network and frontostriatal pathway with regards to task familiarity. *Eur. J. Neurosci.* 2015; **41**: 835–844.
14. Fox MD, Snyder AZ, Vincent JL, Raichle ME. Intrinsic fluctuations within cortical systems account for intertrial variability in human behavior. *Neuron* 2007; **56**: 171–184.
15. Fatouros-Bergman H, Cervenka S, Flyckt L, Edman G, Farde L. Meta-analysis of cognitive performance in drug-naive patients with schizophrenia. *Schizophr. Res.* 2014; **158**: 156–162.
16. Unschuld PG, Buchholz AS, Varvaris M *et al.* Prefrontal brain network connectivity indicates degree of both schizophrenia risk and cognitive dysfunction. *Schizophr. Bull.* 2014; **40**: 653–664.
17. Wu G, Wang Y, Mwansisya TE *et al.* Effective connectivity of the posterior cingulate and medial prefrontal cortices relates to working memory impairment in schizophrenic and bipolar patients. *Schizophr. Res.* 2014; **158**: 85–90.
18. Fingelkurts AA, Fingelkurts AA, Kähkönen S. Functional connectivity in the brain--is it an elusive concept? *Neurosci. Biobehav. Rev.* 2005; **28**: 827–836.
19. Varela F, Lachaux JP, Rodriguez E, Martinerie J. The BrainWeb: Phase synchronization and large-scale integration. *Nat. Rev. Neurosci.* 2001; **2**: 229–239.
20. Rubinov M, Sporns O. Complex network measures of brain connectivity: Uses and interpretations. *Neuroimage* 2010; **52**: 1059–1069.
21. Achard S, Bullmore E. Efficiency and cost of economical brain functional networks. *PLoS Comput. Biol.* 2007; **3**: e17.
22. Stam CJ, Reijneveld JC. Graph theoretical analysis of complex networks in the brain. *Nonlinear Biomed. Phys.* 2007; **1**: 3.
23. Brookes MJ, Woolrich M, Luckhoo H *et al.* Investigating the electrophysiological basis of resting state networks using magnetoencephalography. *Proc. Natl. Acad. Sci. U. S. A.* 2011; **108**: 16783–16788.
24. Hipp JF, Hawellek DJ, Corbetta M, Siegel M, Engel AK. Large-scale cortical correlation structure of spontaneous oscillatory activity. *Nat. Neurosci.* 2012; **15**: 884–890.
25. Sunaga M, Takei Y, Kato Y *et al.* Frequency-specific resting connectome in bipolar disorder: An MEG study. *Front. Psychiatry* 2020; **11**: 597.
26. Kato Y, Takei Y, Umeda S, Mimura M, Fukuda M. Alterations of heartbeat evoked magnetic fields induced by sounds of disgust. *Front. Psychiatry* 2020; **11**: 683.
27. Grent-'t-Jong T, Gross J, Goense J *et al.* Resting-state gamma-band power alterations in schizophrenia reveal E/I-balance abnormalities across illness-stages. *Elife* 2018; **7**: e37799.
28. Chen CM, Stanford AD, Mao X *et al.* GABA level, gamma oscillation, and working memory performance in schizophrenia. *Neuroimage Clin.* 2014; **4**: 531–539.
29. Takei Y, Fujihara K, Tagawa M *et al.* The inhibition/excitation ratio related to task-induced oscillatory modulations during a working memory task: A multtimodal-imaging study using MEG and MRS. *Neuroimage* 2016; **128**: 302–315.
30. Ohki T, Matsuda T, Gunji A *et al.* Timing of phase-amplitude coupling is essential for neuronal and functional maturation of audiovisual integration in adolescents. *Brain Behav.* 2020; **10**: e01635.
31. Ohki T, Gunji A, Takei Y *et al.* Neural oscillations in the temporal pole for a temporally congruent audio-visual speech detection task. *Sci. Rep.* 2016; **6**: 37973.
32. Hinkley LB, Vinogradov S, Guggisberg AG, Fisher M, Findlay AM, Nagarajan SS. Clinical symptoms and alpha band resting-state functional connectivity imaging in patients with schizophrenia: Implications for novel approaches to treatment. *Biol. Psychiatry* 2011; **70**: 1134–1142.
33. Bowyer SM, Gjini K, Zhu X *et al.* Potential biomarkers of schizophrenia from MEG resting-state functional connectivity networks: Preliminary data. *J. Behav. Brain Sci.* 2015; **05**: 1–11.
34. Robinson SE, Mandell AJ. Mutual information in a MEG complexity measure suggests regional hyper-connectivity in schizophrenic probands. *Neuropsychopharmacology* 2015; **40**: 251–252.
35. Zhang X, Wang YT, Wang Y *et al.* Ultra-slow frequency bands reflecting potential coherence between neocortical brain regions. *Neuroscience* 2015; **289**: 71–84.
36. Houck JM, Çetin MS, Mayer AR *et al.* Magnetoencephalographic and functional MRI connectomics in schizophrenia via intra- and inter-network connectivity. *Neuroimage* 2017; **145**: 96–106.

37. Rutter L, Nadar SR, Holroyd T *et al*. Graph theoretical analysis of resting magnetoencephalographic functional connectivity networks. *Front. Comput. Neurosci.* 2013; **7**: 93.

38. Oldfield RC. The assessment and analysis of handedness: The Edinburgh inventory. *Neuropsychologia* 1971; **9**: 97–113.

39. First MB Sr, Gibbon M, Williams JBW. *Structured Clinical Interview for DSM-IV Axis I Disorders. Clinician 2.0 Version*. New York State Psychiatric Institute, New York, 1996.

40. First MBGM, Spitzer RL, Williams JBW, Benjamin LS. *Structured Clinical Interview for DSM-IV Axis II Personality Disorders (SCID-II) User's Guide and Interview*. American Psychiatric Press, Washington, DC, 1997.

41. Kay SR, Fiszbein A, Opler LA. The Positive and Negative Syndrome Scale (PANSS) for schizophrenia. *Schizophr. Bull.* 1987; **13**: 261–276.

42. Matsuoka K, Kim Y, Hiro H *et al*. Development of Japanese Adult Reading Test (JART) for predicting premorbid IQ in mild dementia. *Seishin Igaku* 2002; **44**: 503–511.

43. Hall RC. Global assessment of functioning. A modified scale. *Psychosomatics* 1995; **36**: 267–275.

44. Inada T, Inagaki A. Psychotropic dose equivalence in Japan. *Psychiatry Clin. Neurosci.* 2015; **69**: 440–447.

45. Hoddes E, Dement WC, Zarcone V. The history and use of the Stanford sleepiness scale. *Psychophysiology* 1971; **9**: 150.

46. Taulu S, Simola J. Spatiotemporal signal space separation method for rejecting nearby interference in MEG measurements. *Phys. Med. Biol.* 2006; **51**: 1759–1768.

47. Taulu S, Kajola M, Simola J. Suppression of interference and artifacts by the signal space separation method. *Brain Topogr.* 2004; **16**: 269–275.

48. Gramfort A, Luessi M, Larson E *et al*. MNE software for processing MEG and EEG data. *Neuroimage* 2014; **86**: 446–460.

49. Dale AM, Fischl B, Sereno MI. Cortical surface-based analysis. I. Segmentation and Surface Reconstruction. *Neuroimage* 1999; **9**: 179–194.

50. Fischl B, Sereno MI, Dale AM. Cortical surface-based analysis. II: Inflation, flattening, and a surface-based coordinate system. *Neuroimage* 1999; **9**: 195–207.

51. Reuter M, Schmansky NJ, Rosas HD, Fischl B. Within-subject template estimation for unbiased longitudinal image analysis. *Neuroimage* 2012; **61**: 1402–1418.

52. Hämäläinen MS, Sarvas J. Realistic conductivity geometry model of the human head for interpretation of neuromagnetic data. *IEEE Trans. Biomed. Eng.* 1989; **36**: 165–171.

53. Lin FH, Witzel T, Ahlfors SP, Stufflebeam SM, Belliveau JW, Hämäläinen MS. Assessing and improving the spatial accuracy in MEG source localization by depth-weighted minimum-norm estimates. *Neuroimage* 2006; **31**: 160–171.

54. O'Neill GC, Barratt EL, Hunt BA, Tewari PK, Brookes MJ. Measuring electrophysiological connectivity by power envelope correlation: A technical review on MEG methods. *Phys. Med. Biol.* 2015; **60**: R271–R295.

55. Mostame P, Sadaghiani S. Phase- and amplitude-coupling are tied by an intrinsic spatial organization but show divergent stimulus-related changes. *Neuroimage* 2020; **219**: 117051.

56. Deco G, Corbetta M. The dynamical balance of the brain at rest. *Neuroscientist* 2011; **17**: 107–123.

57. Colclough GL, Woolrich MW, Tewarie PK, Brookes MJ, Quinn AJ, Smith SM. How reliable are MEG resting-state connectivity metrics? *Neuroimage* 2016; **138**: 284–293.

58. Khan S, Hashmi JA, Mamashli F *et al*. Maturation trajectories of cortical resting-state networks depend on the mediating frequency band. *Neuroimage* 2018; **174**: 57–68.

59. Roopun AK, Cunningham MO, Racca C, Alter K, Traub RD, Whittington MA. Region-specific changes in gamma and beta2 rhythms in NMDA receptor dysfunction models of schizophrenia. *Schizophr. Bull.* 2008; **34**: 962–973.

60. Bassett DS, Bullmore E. Small-world brain networks. *Neuroscientist* 2006; **12**: 512–523.

61. Bullmore E, Sporns O. Complex brain networks: Graph theoretical analysis of structural and functional systems. *Nat. Rev. Neurosci.* 2009; **10**: 186–198.

62. Watts DJ, Strogatz SH. Collective dynamics of 'small-world' networks. *Nature* 1998; **393**: 440–442.

63. Latora V, Marchiori M. Efficient behavior of small-world networks. *Phys. Rev. Lett.* 2001; **87**: 198701.

64. Jones E, Oliphant T & Peterson P. SciPy: Open source scientific tools for python. 2001. Available from URL: http://www.scipy.org/, cited date, September, 24, 2020.

65. Genovese CR, Lazar NA, Nichols T. Thresholding of statistical maps in functional neuroimaging using the false discovery rate. *Neuroimage* 2002; **15**: 870–878.

66. Liu Y, Liang M, Zhou Y *et al*. Disrupted small-world networks in schizophrenia. *Brain* 2008; **131**: 945–961.

67. Lynall ME, Bassett DS, Kerwin R *et al*. Functional connectivity and brain networks in schizophrenia. *J. Neurosci.* 2010; **30**: 9477–9487.

68. Anderson A, Cohen MS. Decreased small-world functional network connectivity and clustering across resting state networks in schizophrenia: An fMRI classification tutorial. *Front. Hum. Neurosci.* 2013; **7**: 520.

69. Wang LX, Guo F, Zhu YQ *et al*. Effect of second-generation antipsychotics on brain network topology in first-episode schizophrenia: A longitudinal rs-fMRI study. *Schizophr. Res.* 2019; **208**: 160–166.

70. Alexander-Bloch A, Lambiotte R, Roberts B, Giedd J, Gogtay N, Bullmore E. The discovery of population differences in network community structure: New methods and applications to brain functional networks in schizophrenia. *Neuroimage* 2012; **59**: 3889–3900.

71. Micheloyannis S, Pachou E, Stam CJ *et al*. Small-world networks and disturbed functional connectivity in schizophrenia. *Schizophr. Res.* 2006; **87**: 60–66.

72. Sakkalis V, Oikonomou T, Pachou E, Tollis I, Micheloyannis S, Zervakis M. Time-significant wavelet coherence for the evaluation of schizophrenic brain activity using a graph theory approach. *Annual International Conference of the IEEE Engineering in Medicine and Biology Society 2006*. New York. 2006; 4265–4268.

73. Rubinov M, Knock SA, Stam CJ *et al*. Small-world properties of nonlinear brain activity in schizophrenia. *Hum. Brain Mapp.* 2009; **30**: 403–416.

74. Adler CM, Goldberg TE, Malhotra AK, Pickar D, Breier A. Effects of ketamine on thought disorder, working memory, and semantic memory in healthy volunteers. *Biol. Psychiatry* 1998; **43**: 811–816.

75. Moghaddam B. Bringing order to the glutamate chaos in schizophrenia. *Neuron* 2003; **40**: 881–884.

76. Pilowsky LS, Bressan RA, Stone JM *et al*. First in vivo evidence of an NMDA receptor deficit in medication-free schizophrenic patients. *Mol. Psychiatry* 2006; **11**: 118–119.

77. Akbarian S, Sucher NJ, Bradley D *et al*. Selective alterations in gene expression for NMDA receptor subunits in prefrontal cortex of schizophrenics. *J. Neurosci.* 1996; **16**: 19–30.

78. Sanfratello L, Houck JM, Calhoun VD. Relationship between MEG global dynamic functional network connectivity measures and symptoms in schizophrenia. *Schizophr. Res.* 2019; **209**: 129–134.

79. Zeev-Wolf M, Levy J, Jahshan C *et al*. MEG resting-state oscillations and their relationship to clinical symptoms in schizophrenia. *Neuroimage Clin.* 2018; **20**: 753–761.

80. Schoffelen JM, Gross J. Source connectivity analysis with MEG and EEG. *Hum. Brain Mapp.* 2009; **30**: 1857–1865.

81. de Pasquale F, Della Penna S, Snyder AZ *et al*. Temporal dynamics of spontaneous MEG activity in brain networks. *Proc. Natl. Acad. Sci. U. S. A.* 2010; **107**: 6040–6045.

82. Hironaga N, Takei Y, Mitsudo T, Kimura T, Hirano Y. Prospects for future methodological development and application of magnetoencephalography devices in psychiatry. *Front. Psych.* 2020; **11**: 863.

83. Sekihara K, Owen JP, Trisno S, Nagarajan SS. Removal of spurious coherence in MEG source-space coherence analysis. *IEEE Trans. Biomed. Eng.* 2011; **58**: 3121–3129.

84. Schroeder CE, Lakatos P, Kajikawa Y, Partan S, Puce A. Neuronal oscillations and visual amplification of speech. *Trends Cogn. Sci.* 2008; **12**: 106–113.

85. Jin SH, Seol J, Kim JS, Chung CK. How reliable are the functional connectivity networks of MEG in resting states? *J. Neurophysiol.* 2011; **106**: 2888–2895.

86. Miraglia F, Vecchio F, Bramanti P, Rossini PM. EEG characteristics in "eyes-open" versus "eyes-closed" conditions: Small-world network architecture in healthy aging and age-related brain degeneration. *Clin. Neurophysiol.* 2016; **127**: 1261–1268.

87. Palva JM, Wang SH, Palva S *et al*. Ghost interactions in MEG/EEG source space: A note of caution on inter-areal coupling measures. *Neuroimage* 2018; **173**: 632–643.

88. Farahibozorg SR, Henson RN, Hauk O. Adaptive cortical parcellations for source reconstructed EEG/MEG connectomes. *Neuroimage* 2018; **169**: 23–45.

Supporting information

Additional Supporting Information may be found in the online version of this article at the publisher's web-site:

Appendix S1 Supporting information

Fig. S1. The median correlation matrices of the HC and SZ groups.

Fig. S2. The histogram of correlation values of the HC and SZ groups.

Fig. S3. The distribution of z-scores of the C-COEF at each frequency band at the threshold of 20%.

Table S1. Correlation values and total number of edges at each threshold.

Table S2. DG-CENT at each threshold and frequency band.

Table S3. C-COEF at each threshold and frequency band.

Table S4. GLOB-E at each threshold and frequency band.

Table S5. LOC-E at each threshold and frequency band.

Table S6. SWN at each threshold and frequency band.